Evolution of large eddies in compressible shear layers

Dimitri Papamoschou and Asi Bunyajitradulya

Citation: Physics of Fluids (1994-present) **9**, 756 (1997); doi: 10.1063/1.869230
View online: http://dx.doi.org/10.1063/1.869230
View Table of Contents: http://scitation.aip.org/content/aip/journal/pof2/9/3?ver=pdfcov
Published by the AIP Publishing

Evolution of large eddies in compressible shear layers

Dimitri Papamoschou and Asi Bunyajitradulya
Department of Mechanical and Aerospace Engineering, University of California, Irvine, California 92717

(Received 15 July 1996; accepted 7 November 1996)

The evolution of large turbulent eddies has been investigated in seven supersonic shear layers with average convective Mach numbers $\overline{M_c}$ ranging from 0.22 to 0.86 and with large variation in density and velocity ratios. A two-laser, single-detector planar laser-induced fluorescence technique was used to visualize the flow and its evolution. Two-dimensional pattern matching yielded the convective velocity of the eddies. For $\overline{M_c}>0.3$, fast and slow modes of eddy propagation were detected in supersonic–subsonic and supersonic–supersonic combinations, respectively. An empirical model for the convective velocity is proposed. Plan views reveal coexistence of two- and three-dimensional disturbances. Interaction among eddies appears significantly suppressed. The findings have direct impact on supersonic jet noise and are very relevant to supersonic combustion.
 [S1070-6631(97)00703-4]

I. INTRODUCTION

The role of large eddies, or ''coherent structures,'' is central in the investigation of turbulence in practical systems. Since the subsonic shear-layer experiments of Brown and Roshko[1] the fluid-mechanics community has come to accept the fact that large-scale motions are an inseparable feature of turbulent shear flows. For subsonic flows, it has been shown by numerous works that large eddies are principally responsible for fluid entrainment into the mixing region. The remarkable similarities between the quasi-deterministic behavior of large eddies and the predictions of linear stability theory lend credence to the notion that large eddies represent the most amplified instability of the flow.[2] Although large eddies are obvious in visualizations, it is difficult to attribute to them a universal description. Definition depends to some extent on the means and goals of the investigation. Perhaps the most specific one, proposed by Hussain,[3] treats the coherent structure as ''a connected turbulent fluid mass with instantaneously phase-correlated vorticity over its spatial extent.'' In this paper we use a similar—albeit less rigorous—definition which centers on the phase-correlated field of a passive scalar.

In compressible shear flows, the role of large eddies is more perplexing. Before discussing it, let us first define a key compressibility parameter, the convective Mach number. Referring to Fig. 1, it is the Mach number of the dominant flow instability with respect to either freestream of the shear layer; thus it takes two values:

$$M_{c_1}=\frac{U_1-U_c}{a_1},\qquad M_{c_2}=\frac{U_c-U_2}{a_2}, \tag{1}$$

where U_c is the phase speed of the instability. This concept of an instability Mach number was introduced by Mack[4] in his linearized treatment of compressible boundary layers. Later, it was proposed as a compressibility parameter for turbulent shear layers,[5,6] with U_c representing the eddy convective velocity. A ''symmetric'' Lagrangian model for the large structure,[6] whereby the two freestreams suffer equal total-pressure loss as they are entrained towards a stagnation point inside the mixing region, gives

$$M_{c_1}\approx M_{c_2}\approx\frac{\Delta U}{a_1+a_2}. \tag{2}$$

The corresponding dimensionless convective velocity is

$$\frac{U_c-U_2}{U_1-U_2}=\frac{1}{1+\sqrt{\rho_2/\rho_1}}. \tag{3}$$

Even though the prediction of Eq. (2) may be inaccurate for high compressibility, the ''average'' convective Mach number $\overline{M_c}=\Delta U/(a_1+a_2)$ is still a useful measure of overall shear-layer compressibility and will be used as such in this paper.

Experiments on the turbulent structure of compressible shear layers agree widely on two key points. First, the growth rate declines with increasing $\overline{M_c}$, with similar reductions in the turbulent fluctuating velocities and shear stresses.[6–8] Second, turbulence becomes more disorganized, with less two-dimensional coherence, as $\overline{M_c}$ exceeds a value of around 0.5.[9] Linear stability theory and direct numerical simulation predict the growth-rate suppression quite well (see for example Refs. 10 and 11). Theory and simulation also predict that, above a certain $\overline{M_c}$, three-dimensional disturbances are more unstable than two-dimensional ones.[12,13] On the surface, this correlates with the increased three-dimensionality observed experimentally.[9] Note, however, that analyses and computations typically impose a certain wave obliquity and examine its effect on the growth rate; the possibility of co-existence of waves of different obliquities, and investigation of their interactions, is seldom explored.

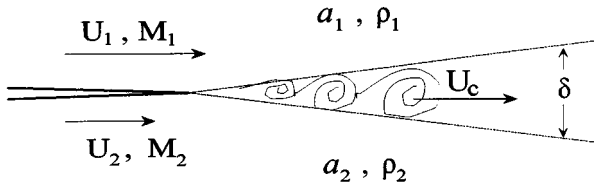

FIG. 1. Shear-layer geometry and nomenclature.

 1070-6631/97/9(3)/756/10/$10.00

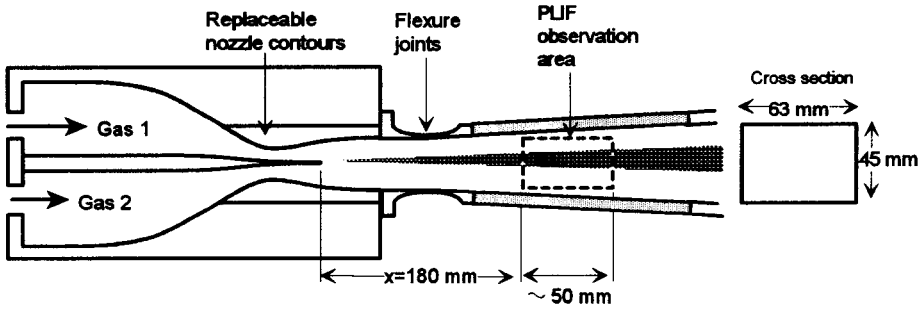

FIG. 2. Test-section schematic.

Another central area of compressible turbulence—where less agreement is found—deals with the evolution of eddies and in particular with their convective velocity U_c. The convective velocity is important because it influences entrainment into the mixing region[14] and has direct impact on supersonic jet noise.[15] Double-exposure schlieren observations of shear layers by Papamoschou,[16] covering ten flow cases, showed nearly ''frozen'' patterns convecting with velocities very different from those predicted by Eq. (3). In layers composed of two supersonic streams, eddies traveled with a velocity close to that of the slow freestream (slow modes) while in supersonic–subsonic layers they traveled with a velocity close to that of the fast freestream (fast modes). Fast modes were subsequently observed by Fourguette *et al.*[17] who used planar Mie scattering and two-dimensional cross-correlations to track eddies at the edge of a supersonic jet (one case). In the work by Hall *et al.*,[18] fast modes were detected by correlation of wall pressure traces, created by Mach waves, in a supersonic–subsonic shear layer. It is noteworthy that fast and slow modes are also found in stability analysis of supersonic shear layers and jets.[19,20] On the other hand, a recent study of supersonic–subsonic shear layers by Elliott *et al.*[21] (two cases), using product formation and one-dimensional space-time correlations, concluded that U_c is a function of transverse position and is roughly equal to the local mean velocity. A similar result was found in a reacting experiment by Seitzman *et al.*,[22] where the edges of the shear layer were visualized using OH/acetone fluorescence.

Clearly, our understanding of compressible eddies is still lacking. The purpose of this study is to examine the evolution of shear-layer turbulence using diagnostic and analysis tools that we believe capture the nature of large eddies. We focus on the most dominant instability, which—in similarity to the subsonic experience—we assume takes the form of large vortical structures. We use a slowly diffusing passive scalar to visualize, at least approximately, the streamline patterns responsible for entrainment of that scalar from the freestream into the vortical core. We define large eddies as phase-correlated two-dimensional patterns of that passive scalar, the size of the pattern being of the same order as the local thickness of the shear layer. Phase correlation is done by a 2D pattern matching technique which yields the convective velocity of the eddies. At the same time, we observe the level of interaction between eddies and characterize their three-dimensionality. We cover a variety of shear layers encompassing supersonic–subsonic and the less-investigated supersonic–supersonic combinations.

II. FACILITY AND DIAGNOSTICS

Experiments were performed in the UCI Supersonic Turbulence Laboratory. The facility used is a two-stream, blow-down wind tunnel in which a variety of gases and Mach numbers can be selected to form a shear layer (Fig. 2). At the measurement location the test section is 45 mm high and 63 mm wide. Optical access is provided by quartz windows on all four walls of the test section. The downstream side of the test section is connected to a low-pressure dump tank connected to a vacuum pump. Gaseous acetone can be seeded in either of the shear-layer streams. Injection is accomplished by supplying liquid acetone at high pressure through atomizing nozzles placed 1.5 m upstream of the settling chamber. The flow of gases and acetone is controlled by solenoid and pressure-regulating valves. Pressure transducers recorded the static-pressure distribution on the upper and lower test-section walls and the total pressures of each stream.

The diagnostic technique used to visualize the turbulent structure and its evolution is summarized in Fig. 3. The tech-

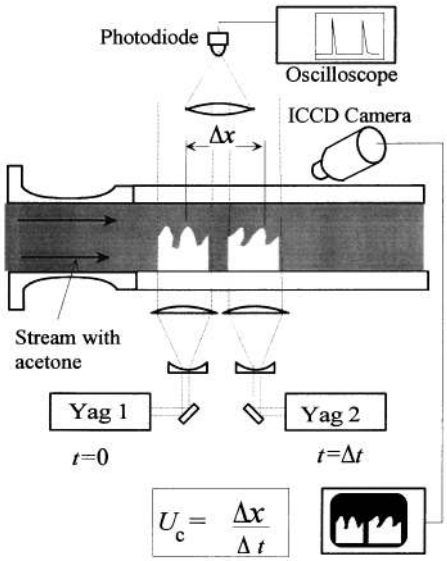

FIG. 3. Double/offset-exposure PLIF used for study of eddy evolution.

TABLE I. Test parameters and results (velocities in m/s).

Case	$\overline{M_c}$	Gas1	Gas2	M_1	M_2	$\frac{\rho_2}{\rho_1}$	U_1	U_2	U_c [a]	U_c	M_{c_1}	M_{c_2}
N22A21	0.22	Air	Argon	2.0	2.1	1.78	530	425	470	470	0.22	0.25
N15N03	0.52	Air	Air	1.5	0.3	0.72	430	120	281	345	0.26	0.67
N15N03P	0.52	Air	Air	1.5	0.3	0.72	430	120	281	389	0.15	0.83
N14A02	0.54	Air	Argon	1.4	0.2	1.03	390	70	229	333	0.21	0.84
N20N04	0.63	Air	Air	2.0	0.4	0.58	500	130	339	462	0.15	1.00
H15N16	0.67	Helium	Air	1.5	1.6	6.26	1130	440	639	462	0.89	0.07
H19N20	0.83	Helium	Air	2.0	1.9	5.85	1280	500	731	536	1.10	0.13
H16N08	0.86	Helium	Air	1.6	0.8	4.46	1170	250	546	724	0.60	1.47

[a]Equation (3).

nique is based on laser-induced fluorescence of acetone, a comprehensive discussion of which can be found in Lozano *et al.*[23] Gaseous acetone, at mole fractions around 1%, was seeded in one of the shear-layer streams. Two adjacent laser sheets, generated by the fourth harmonic (266 nm) outputs of two independently pulsed Nd:YAG lasers (Continuum Surelite II) sliced the shear layer. At the test section, each laser sheet was 0.3 mm thick and about 30 mm wide; pulse energies were approximately 20 mJ. The ultraviolet sheets excited the acetone molecules which fluoresced in the visible range ($\lambda \approx 480$ nm), thus marking the seeded fluid. The upstream sheet was triggered first, and the downstream sheet second with a time delay Δt. Both sheets were imaged onto a single detector (Princeton Instruments ICCD 576S/RB). By adjusting Δt, the evolution of a turbulent feature seen in the first sheet was captured in the second sheet. Cross-correlations, discussed later, yielded the distance Δx traveled by identifiable features. The convective velocity was then computed by $U_c = \Delta x/\Delta t$. Precise synchronization of the lasers and camera with the solenoid valves was achieved using a data acquisition/control system on a 486DX-66 computer. The time delay between the two lasers was independently confirmed by a photodiode placed in the path of the sheets exiting the test section.

III. EXPERIMENTAL CONDITIONS

The double/offset-exposure PLIF technique was applied at an axial location $x = 180$ mm downstream of the splitter plate. The corresponding non-dimensional distance was $x/\theta \approx 2000$, where θ is the calculated boundary-layer momentum thickness of the fast stream at the edge of the splitter plate; thus we believe the flow to be fully developed at the measurement location. Static pressures were around 40 kPa and the typical Reynolds number based on shear-layer thickness was 2×10^5. The total pressures were set such that the shear layers were pressure matched. To prevent choking of the flow and to provide near-zero pressure gradients, the upper and lower test section walls diverged at a combined angle of 3°.

Mach numbers at the measurement location ($x = 180$ mm) were inferred from measurements of the total pressures and of the local wall static pressure; they are close to the nominal values associated with the nozzle blocks of Mach 1.5 and Mach 2.0. Table I lists the conditions for the eight cases we investigated, in order of increasing $\overline{M_c}$. For ease of reference, each case is assigned a name consisting of a code for the gases (N for air, A for argon, H for helium) and their Mach numbers. For example, case H16N08 means helium at Mach 1.6 and air at Mach 0.8. Case N15N03P is the same as N15N03, only the visualizations are plan views. Alternating (fast-stream and slow-stream) injection of acetone was performed for cases N22A21, N15N03, N14A02, H15N16, and H16N08. In the remaining cases, acetone was injected in the fast stream.

IV. CROSS-CORRELATION METHOD

As mentioned in the Introduction, we define and track an eddy using the two-dimensional cross-correlation of a passive scalar, in this case acetone concentration $c(x,y,t)$. A spatial pattern of acetone signal is distinguished from the background by the fluctuation $c'(x,y,t) = c(x,y,t) - \langle c(x,y,t) \rangle$, where $\langle\ \rangle$ denotes the spatial average. Consider two realizations of an $L_x \times L_y$ pattern, one at $t = 0$ and the other at $t = \Delta t$. The two-dimensional cross-correlation of the two realizations is

$$C(\xi,\eta,\Delta t) = \frac{1}{L_x L_y} \int_0^{L_y} \int_0^{L_x} c'(x+\xi, y+\eta, \Delta t) \times c'(x,y,0)\,dx\,dy. \tag{4}$$

The extension of Eq. (4) to our images is outlined in Fig. 4. We define an image field $F(\xi,\eta)$, typically the entire image. Recall that the left half of F corresponds to $t = 0$ and the right half to $t = \Delta t$. In the left half of F, we select a template

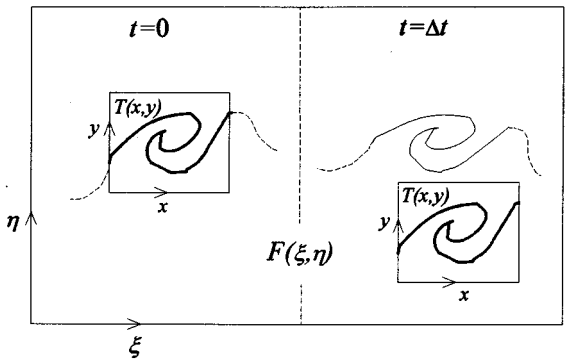

FIG. 4. Illustration of 2D cross-correlation method. Template $T(x,y)$ containing turbulent feature slides over entire image field $F(\xi,\eta)$.

$T(x,y)$, of size $M \times N$, containing the pattern of interest (x, y, ξ, and η are treated now as integers). The template slides in both directions over the entire image field, and the following correlation is computed:

$$C_{TF}(\xi,\eta)=\frac{1}{MN}\sum_{\xi=0}^{M}\sum_{\eta=0}^{N} T'(x,y)F'(x+\xi,y+\eta), \quad (5)$$

where $T'=T-\langle T\rangle$ and $F'=F-\langle F\rangle$, $\langle\ \rangle$ denoting the spatial average over the $M \times N$ region of the template and of the overlapping image field. When T' slides on the right half of the image ($t=\Delta t$), Eq. (5) becomes a space-time correlation in two dimensions. The correlation coefficient is defined as

$$R_{TF}(\xi,\eta)=\frac{C_{TF}(\xi,\eta)}{\sqrt{C_{FF}(\xi,\eta)C_{TT}}} \quad (6)$$

and takes the value of 1.0 for perfect correlation, i.e., when the template overlaps with itself. Typical template sizes were $M=N=150$ pixels, while the image field was as large as 384 $\times$576 pixels. The cross-correlation procedure is computationally intensive, each correlation taking an average of five hours to process on a Pentium 100 computer.

To assess the sensitivity of results on choice of template, we performed cross-correlations on the same image using nine different template sizes and locations, each template containing a sizable portion of the turbulent feature of interest. This was done for one image of each of the eight cases examined. The resulting standard deviation in the U_c measurement was 5% or less. For each flow case, we cross-correlated an average of ten images. The standard deviation of U_c from one image to the other was also around 5%, the highest value being 7% for case N15N03P. We conclude, therefore, that the uncertainty in the reported values U_c, for all the cases, is no larger than 7%. For each case, we never noticed an excursion of U_c beyond that uncertainty.

This correlation procedure amounts to phase alignment between the structure at $t=0$ and its evolution at $t=\Delta t$. That is, to compute the convective velocity, we set a criterion based on the shape of the original structure which we try to match at a later time. However, that criterion changes from one image pair to the next. The resulting definition of eddies is thus similar to Hussain's,[3] who used certain features of the vorticity field as a criterion to define coherent structures, but less rigorous since our criterion changes while Hussain's remained constant.

V. RESULTS

In the course of our investigation, we have obtained a large number of PLIF images which are single- or double-exposure. We have seen consistently the presence of large structures. They appear to be an inseparable feature of the flow, even though at high $\overline{M_c}$ their shape can vary significantly from one picture to the next. In some of the double-exposure images we cannot track features because we used too long or too short a Δt in the method of Fig. 3, an unavoidable part of the experimentation process.

Approximately two hundred images with large-scale features that can be followed from the first sheet to the next have been collected. In all these images, one can make

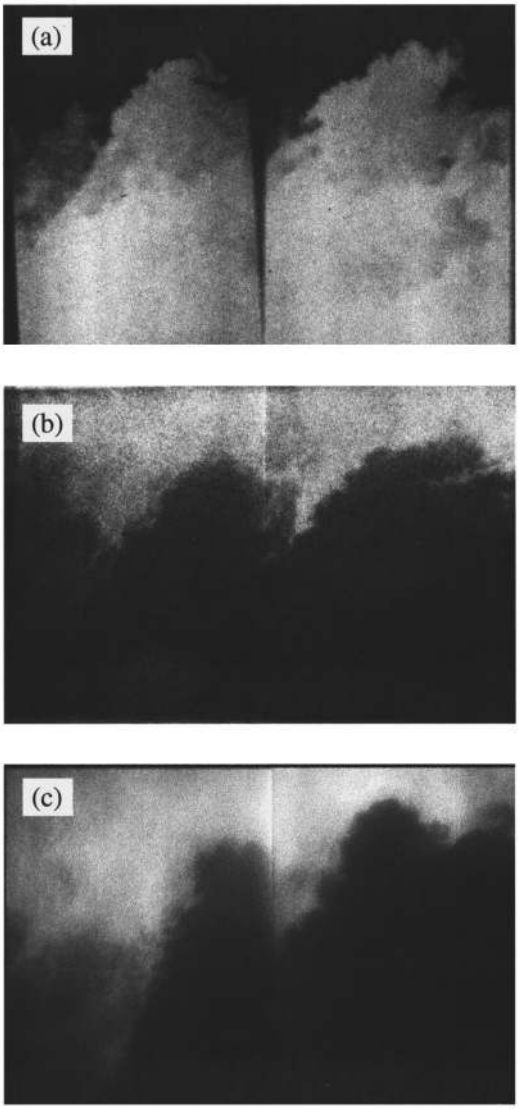

FIG. 5. Selected images of supersonic-subsonic cases: (a) N15N03 with acetone seeded in slow stream (FOV=65 mm, $\Delta t=70$ μs); (b) N15N03 with acetone seeded in fasts stream (FOV=65 mm, $\Delta t=70$ μs); (c) N14A02 (FOV=51 mm, $\Delta t=65$ μs).

''manual'' U_c measurements by following with the eye identifiable features.[24] Eighty one of these images have been cross-correlated, i.e., an average of ten images for each flow case. Selection of an image for cross-correlation was based on factors such as uniformity of lighting and lack of spots, not the ability to identify trackable features. The U_c values from cross-correlations and from manual measurements are very close. However, only the cross-correlation values are included in this paper. The images are presented with the fast stream always on top. The stream seeded with acetone is identified as the bright one.

First we discuss the qualitative features of the flow, starting with the supersonic–subsonic combinations. Figure 5(a) presents a transverse view of case N15N03 ($\overline{M_c}=0.52$), with acetone seeded in the low-speed stream (the term FOV denotes the axial extent of the field of view). The large turbulent features can be easily followed from the first sheet to the second ($\Delta t=70$ μs) though they lack the organized roller-

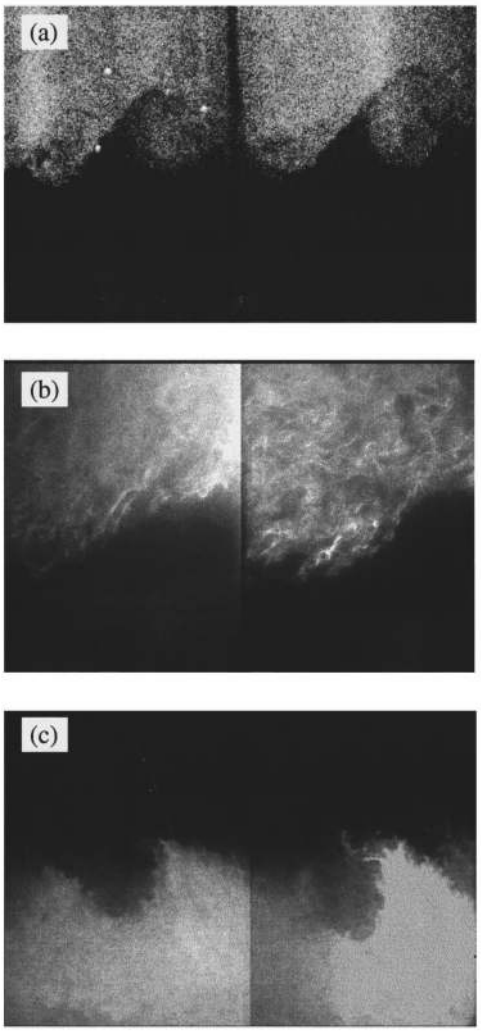

FIG. 6. Selected images of supersonic-supersonic cases: (a) N22A21 (FOV=54 mm, $\Delta t=60$ μs); (b) H15N16 (FOV=51 mm, $\Delta t=55$ μs); (c) H19N20 (FOV=60 mm, $\Delta t=60$ μs).

type structure seen in subsonic experiments (Ref. 1, for example). The eddies deform very slightly, even though they are subjected to significant shear, represented in terms of the eddy roll-over time $\tau=\delta/\Delta U=(0.01\ \text{m})/(320\ \text{m/s})=31$ μs. In other words, within $\Delta t=70$ μs, the eddy should have rotated about twice, yet it appears quite the same. This inertness of the large eddies is a typical feature of the compressible shear layers investigated here. To ensure that our results are not biased on the side in which we seed acetone, we alternated the injection side. Figure 5(b) shows an image of case N15N03 with acetone injected in the high-speed stream. The qualitative features of the flow are the same as before and, as we will see later, the convective velocity measurement is not affected by the injection side. Indeed, acetone appears to mark well the turbulent structure across the entire thickness of the layer. As the convective Mach number increases, eddies become less organized but, because of their inertness, can still be easily followed. Figure 5(c) shows a representative images of case N14A02 ($\overline{M_c}=0.54$).

We now turn to the supersonic–supersonic combinations. Figure 6(a) shows an image of case N22A21 ($\overline{M_c}=0.24$) which has very low compressibility. Even though both freestreams are supersonic, the turbulent structure looks remarkably similar to that observed in subsonic shear layers, that is, organized roller-type structures. As $\overline{M_c}$ increases, the features become less organized. Figures 6(b) and 6(c) show images of cases H15N16 ($\overline{M_c}=0.67$) and H19N20 ($\overline{M_c}=0.83$) where the inert and disorganized nature of the eddies is evident.

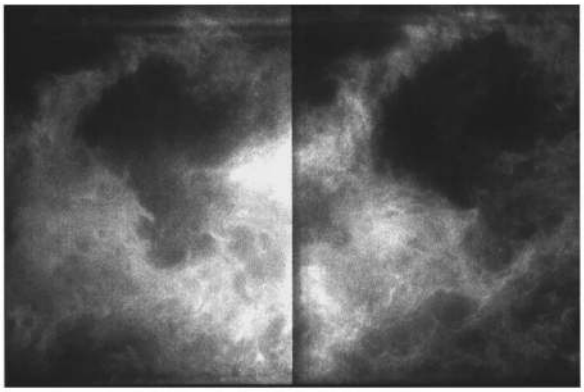

FIG. 7. Example of a plan-view cross section, case N15N03P (FOV=51 mm, $\Delta t=60$ μs).

We acquired plan view images of case N15N03 ($\overline{M_c}=0.48$) by rotating the tunnel 90°, keeping the optics unchanged. The shear layer was sliced at various transverse positions from the low-speed to the high-speed side. Figure 7 shows a typical image at the middle of the layer. The structure is fairly chaotic with no two-dimensional organization. Like its transverse counterpart, it stays nearly frozen from one exposure to the next. There is no significant eddy motion in the spanwise direction, i.e., movement of the structure occurs uniformly in the flow direction. Since the structure is chaotic but propagates frozen, it presents all possible values of obliquity to the freestreams (it helps to think of the structure as a wave front in this respect). In other words, both 2D and 3D disturbances are present. This contrasts with numerical simulations that predict—or impose—that only disturbances of a certain obliquity are present.

We now present the measurements of U_c obtained by the cross-correlation scheme of Eq. (5). Figure 8(a) shows another transverse image of case N15N03 ($\overline{M_c}=0.52$), accompanied by a contour plot of the correlation coefficient $R_{TF}(\xi,\eta)$. The template used for this particular cross-correlation is visible in the image. When the template containing the turbulent eddy matches itself, the correlation coefficient is 1.0. This is seen as the first peak, on the left half of the correlation plot. The second peak on the right half indicates the best match of the template with the evolution of the eddy. The axial distance between the two peaks, Δx, represents the distance traveled by the eddy. The convective velocity is then calculated by $U_c=\Delta x/\Delta t$. In this case, $U_c=377$ m/s, much higher than the value of 281 m/s predicted by Eq. (3). Figure 8(b) shows an example for case H19N20. Here we compute $U_c=547$ m/s, considerably less that the 731 m/s predicted by Eq. (3). For the plan view case

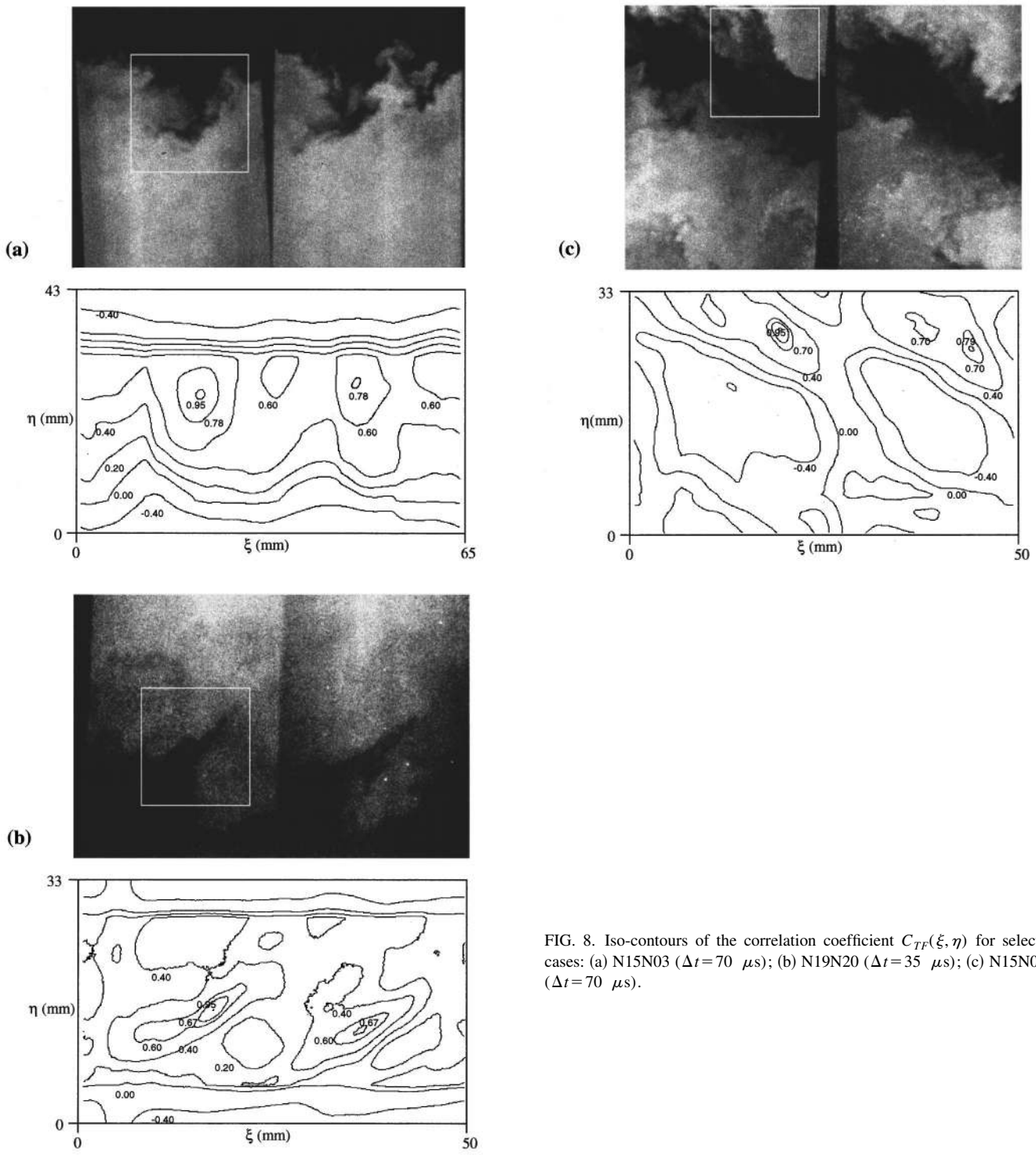

FIG. 8. Iso-contours of the correlation coefficient $C_{TF}(\xi,\eta)$ for selected cases: (a) N15N03 ($\Delta t=70\ \mu$s); (b) N19N20 ($\Delta t=35\ \mu$s); (c) N15N03P ($\Delta t=70\ \mu$s).

N15N03P, seen in Fig. 8(c), the results are close to case N15N03.

Indeed, we confirm trends seen in several previous investigations mentioned in the Introduction: for $\overline{M_c}$ greater than about 0.3, supersonic–subsonic combinations exhibit fast modes and supersonic-supersonic combinations slow modes. The only case where the U_c measurement agrees with Eq. (3) is N22A21 with $\overline{M_c}=0.24$. These observations are illustrated in Fig. 9 where the non-dimensional U_c is plotted versus y (transverse location of template center) for cases N22A21, N15N03, and H15N16. The theoretical prediction of Eq. (3) is superimposed on the plots. For case N22A21 agreement with theory is very good, as expected since this is a low compressibility case. This serves as an additional check on the accuracy of our U_c measurements. In case N15N03, U_c is much higher than the theoretical prediction and in case H15N16 much lower. Figure 9 also shows that the U_c measurement is largely independent of y location

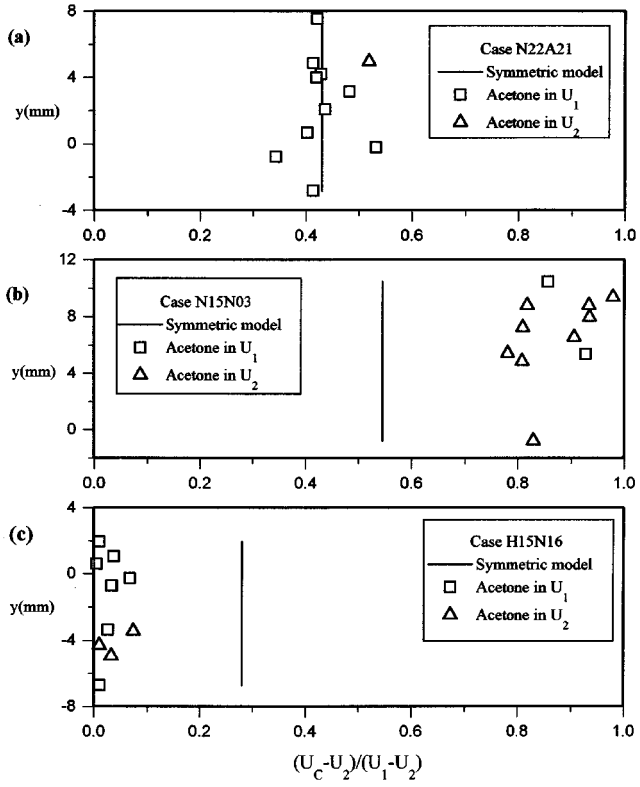

FIG. 9. Normalized U_c versus transverse location of correlation template center for examples of: (a) low-$\overline{M_c}$ case; (b) supersonic–subsonic case; (c) supersonic–supersonic case.

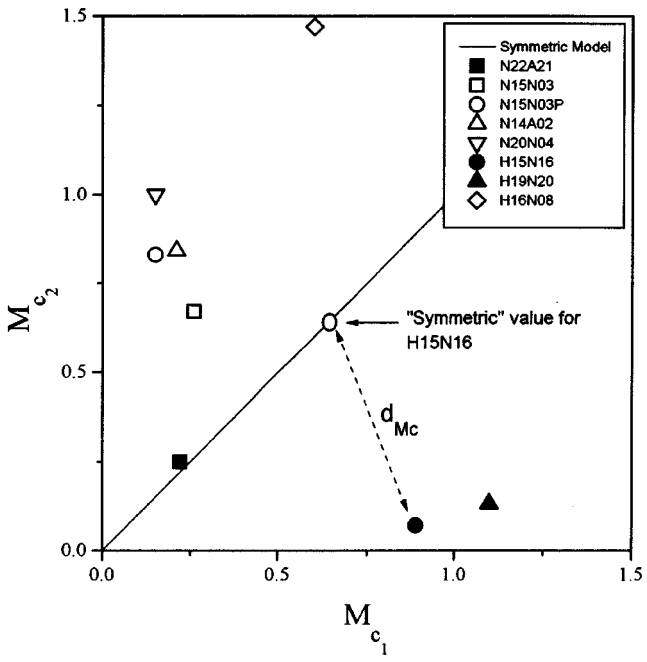

FIG. 10. Convective Mach numbers plotted versus each other: open symbols represent supersonic–subsonic combinations and closed symbol supersonic–supersonic. The d_{M_c} concept for case H15N16 is illustrated.

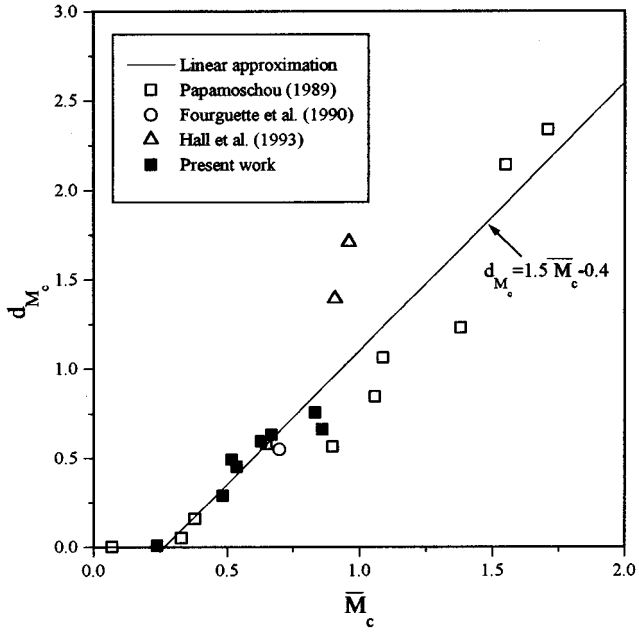

FIG. 11. Convective-Mach-number deviation from symmetric model for present and past works.

and of acetone injection side, supporting our hypothesis that the eddies we track constitute the largest instability of the flow and span the entire thickness of the layer.

We summarize the results in the form of a M_{c_1}-versus-M_{c_2} plot, shown in Fig. 10, where each datum is derived from the average measured value of U_c for a given case. If Eq. (2) were valid, all the points should lie on the diagonal line $M_{c_1}=M_{c_2}$. This happens only for the lowest compressibility case N22A21. All the other cases deviate from the symmetric model according to the trends mentioned previously.

The deviation from the symmetric model can be expressed in terms of the ''distance'' of a measurement from its symmetric value (see Fig. 10)

$$d_{M_c}=\sqrt{(M_{c_1}-\overline{M_c})^2+(M_{c_2}-\overline{M_c})^2} \tag{7}$$

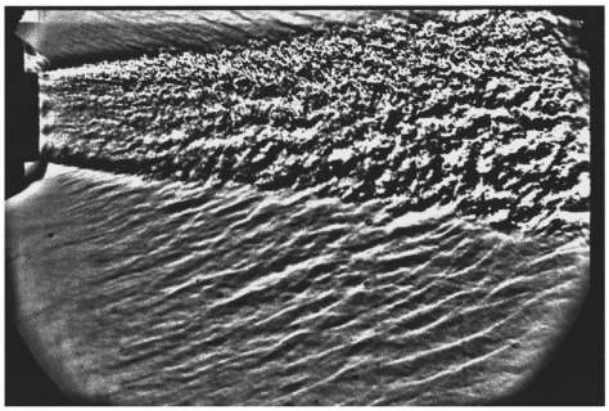

FIG. 12. Schlieren image of a pressure-matched Mach 2 helium jet exhausting into quiescent air at ambient conditions. Mach-wave radiation is prominent.

which is plotted versus $\overline{M_c}$ in Fig. 11. Data of previous investigations that report large-eddy convective velocities are included in the figure. A monotonic trend is observed, which is approximated by the linear fit

$$d_{M_c}=\begin{cases}1.5\overline{M_c}-0.4, & \overline{M_c}>0.27\\ 0, & \overline{M_c}\leqslant 0.27.\end{cases} \tag{8}$$

We can use Eq. (8), together with Eq. (1), to construct an approximate prediction scheme for the convective Mach numbers in the following fashion:

$$\begin{aligned}M_{c_1}&=\overline{M_c}\pm d_{M_c}/\sqrt{1+(a_1/a_2)^2},\\ M_{c_2}&=\overline{M_c}\pm -d_{M_c}/\sqrt{1+(a_2/a_1)^2},\end{aligned} \tag{9}$$

where the plus sign should be used for supersonic–supersonic combinations and the minus sign for supersonic–subsonic combinations.

Applied to flows of practical interest, the above model gives reasonable results. As an example, Fig. 12 presents a schlieren image of a Mach 2 helium jet exhausting into ambient air, obtained in one of our facilities. The jet conditions are $U_1=1330$ m/s, $a_2/a_1=0.53$, and $\overline{M_c}=1.31$. A pattern of Mach waves is evident, generated because the eddies move at supersonic speed with respect to the ambient air. The near field, defined by the potential core surrounded by shear layers, covers the left two thirds of the image. The slope of the Mach waves originating from the near field is approximately 22°, which corresponds to $M_{c_2}\approx 2.7$. This agrees well with the prediction obtained by applying Eq. (8) to Eq. (9), which gives $M_{c_2}=2.69$. It should be understood, however, that at this point the model is entirely empirical. The physical reasons for the asymmetries are yet to be understood.

VI. DISCUSSION

We wish to offer some thoughts on three main issues that arose from this study: the inertness of the large eddies, their asymmetric convective speeds, and the physical meaning of ''convective velocity'' inferred by 2D versus 1D correlations.

Given the sharp decline of growth rates with increasing $\overline{M_c}$, it is not surprising that compressible large eddies are more inert in their mutual interactions than their incompressible counterparts. Previous evolution works have also noticed this inertness at high $\overline{M_c}$.[21] In subsonic flows, large eddies are very active in entrainment and frequently interact with each other, through pairings and amalgamations, to further boost the growth rate. In our images, we do not see evidence of pairing. If it happens, it is probably too slow to be of significance. Recent theoretical works[25,26] have attributed the inactivity of compressible eddies to the reorientation of the pressure field and consequent breakdown in communication between regions of the flow as $\overline{M_c}$ increases. Also, direct numerical simulation of the interaction of vortex filaments has shown that vortex reconnection time is delayed at high Mach numbers, a result of baroclinic and dilatation effects.[27]

The dependence of U_c on whether the freestream velocities are supersonic–supersonic versus supersonic–subsonic is puzzling and cannot be explained by Lagrangian descriptions of the flow. Quantities that are frame-of-reference invariant, like the density ratio and temperature ratio, are inadequate as predictors of which mode will occur. We believe that the answer to this question is tied to the observed inertness of the eddies. If eddies evolve very slowly, where are they formed and where do they acquire their characteristics? A region of special attention should be the trailing edge where the two streams merge. An obvious distinction between supersonic–supersonic and supersonic–subsonic shear layers is that the former have a stronger and more extended wake region than the latter. It is hoped that future experiments will explore the effects of the near field on the morphology and convective velocity of the large eddies.

In previous works,[16,28] it has been speculated that the asymmetric U_c could be the result of a strong shock formed on only one side of the eddy. To satisfy pressure equilibrium at the presumably stable stagnation point between two structures, the stream with the shock would need a much higher M_c than the stream without. While this argument is still plausible for flows with very high $\overline{M_c}$, one has great difficulty extending it to shear layers with $\overline{M_c}$ as low as 0.3–0.5, the apparent threshold for occurrence of asymmetries. It is hard to imagine a process through which fluid in a $\overline{M_c}=0.5$ shear layer accelerates to an M_c on the order of 3 required to cause significant asymmetry. On the other hand, viscous dissipation is strongly related to $\overline{M_c}$ and is significant even at subsonic $\overline{M_c}$'s.[29] Though not as strong locally as the dissipation of a shock, it could produce similar losses if suffered for long distances, i.e., if the streamline leading to the stagnation point has crossed an extended viscous region.

We now comment on the differences between our measurement of U_c, using 2D space-time correlations [Eq. (6)], and the classical measurements that employ 1D correlations in x and t. As mentioned in the Introduction, our research has focused on the largest instability in the flow. Our results indicate that this instability propagates with a single U_c. Elliott *et al.*[21] visualized supersonic–subsonic shear layers ($\overline{M_c}=0.5,0.86$) using double-pulse planar Mie scattering and inferred convective velocities from 1D space-time correlations done simultaneously at many y locations. Specifically, their scheme tracked the convection of a vertical line of signal taken from the initial image and translated in x over the evolution image. Their results indicate that U_c is a function of y and that it basically follows the mean flow velocity. In fact, it appears that all studies using 1D, unconditional space-time correlations come to the same result: the convective velocity is very close to the mean velocity (see for example Refs. 30, 31).

A strong clue as to the relevance of each definition of U_c comes from the flow itself. Consider the phenomenon of Mach wave radiation in supersonic jets and in supersonic–subsonic shear layers (see Fig. 12). It has been observed in flows with $\overline{M_c}$ as low as 0.75[32] and is believed to be a strong contributor to supersonic jet noise.[33] Mach waves are created because a strong instability propagates at supersonic speed

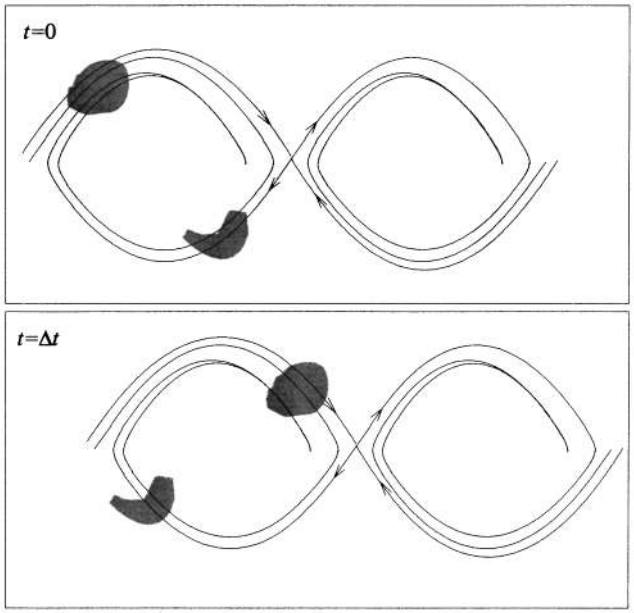

FIG. 13. Illustration of argument that small scales (shown as lumps) travel with convective velocities different from that of the largest eddies.

with respect to the ambient air (or with respect to the low-speed stream in a shear layer). It becomes clear that 1D space-time correlations fail to capture this phenomenon: if U_c followed the mean velocity, the instability would be intrinsically subsonic, hence no Mach waves would be generated. There is little doubt that Mach waves were present in the shear layers of Elliott *et al.*[21] at $\overline{M_c}=0.86$ (the conditions were very similar to those of Hall *et al.*[18] who correlated the pressure traces of Mach waves to infer the convective velocity) yet their U_c measurements do not reflect that. Conversely, the U_c measurements in this paper, inferred by 2D space-time correlations, are consistent with Mach-wave generation.

This does not mean that 1D correlations are inappropriate or invalid. Rather, using 2D versus 1D correlations should depend on the quantity one tries to extract. To obtain the evolution characteristics of large scales, it appears that 2D correlations are more suitable. In an attempt to illustrate this point, we offer the cartoon of Fig. 13. It depicts an idealized view of a large structure in the convective frame and its evolution a short time later. In slowly growing flows, like ours, the mean streamline patterns are nearly closed, indicating little entrainment into the mixing region. So, for a short time, the streamline pattern propagates practically undeformed. At the same time, the streamlines of the large eddies are transporting smaller scales, which in visualizations would appear as patches of the tracer. This superposition of large and small scales has been vividly captured in the shadowgraphs of Brown and Roshko.[1] The small scales travel with a speed close to the local mean value, whereas the large eddy propagates at a constant U_c. One-dimensional, unconditional correlations do not discriminate between large and small scales and cannot capture the two-dimensional extent of the large instability patterns. Since they include the contribution of small scales, the resulting U_c is biased toward the mean flow velocity. Two-dimensional correlations according to Eq. (6) are conditional by their nature. They use a template of integral length scale, thus capture the evolution of the largest eddies and are not significantly affected by the small scales. This scenario explains the differences between our results and those of Elliott *et al.*[21] as well as those Seitzman *et al.*[22] The latter investigation used a fluorescence technique that emphasizes the edges of the shear layer, where tracer patches convect at speeds near the local mean velocity.

Looking at the sketch of Fig. 13, it is evident that the principal Mach wave generator is the large eddy, not the small scales. The large streamline pattern acts like a bumpy wall to the external flow; the small scales travel at a speed close to the local mean velocity, thus they disturb very little the external flow. Is the large eddy as important in entrainment as it is in noise generation? The answer is not clear. Given the slow evolution of eddies, and their lack of interaction, it is questionable if they govern entrainment to the extent seen in subsonic flows. Small scales may be equally important in bringing freestream fluid into the mixing region. This is an issue central to supersonic combustion that needs to be addressed by future works.

VII. CONCLUSIONS

The evolution of large-scale turbulent structures in compressible shear layers has been studied with a laser diagnostic technique which produced cross-sectional digital images of the structure and its evolution. Seven flow cases were studied with convective Mach numbers ranging from 0.22 to 0.86 and with large variations in density and velocity ratios. Two-dimensional cross-correlations were applied to compute the convective velocity of large eddies.

The convective velocity U_c was found to be independent of transverse position. The results were correlated against the ''symmetric'' convective Mach number $\overline{M_c}$. At low $\overline{M_c}$, the measured convective velocity of the large-scale structure is in agreement with the prediction of the symmetric model and eddies appear like their incompressible counterparts. For $\overline{M_c}>0.3$, however, the measurements depart from the symmetric model and two trends become apparent: fast modes, with U_c much higher than the symmetric value; and slow modes, with U_c much lower than the symmetric value. Fast modes were observed exclusively in supersonic–subsonic shear layers, while slow modes occurred only in supersonic–supersonic shear layers. Consequently, the two convective Mach numbers, M_{c_1} and M_{c_2}, are very different from each other, in contrast to the symmetric model that predicts them to be equal. The deviation of M_c's from the symmetric value is a monotonic growing function of $\overline{M_c}$. This leads to an approximate model for predicting the convective Mach numbers.

The appearance of the large-scale structures becomes progressively more disorganized as $\overline{M_c}$ increases, consistent with observations of earlier works. The lack of organization is evident in both side and plan views. The plan views reveal chaotic patterns that present every possible obliquity angle to the freestream flow. The patterns propagate virtually undeformed in a direction aligned with the freestream velocity

vectors. This suggests the coexistence of two- and three-dimensionalities in the flow, an issue of significance for turbulence modeling and for the overall understanding of compressible shear-layer turbulence.

ACKNOWLEDGMENTS

The support by Grants No. CTS-9114220 and CTS-9310830 from the National Science Foundation is gratefully acknowledged.

[1]G. L. Brown and A. Roshko, ''On density effects and large structure in turbulent mixing layers,'' J. Fluid Mech. **64**, 775 (1974).
[2]C. M. Ho and P. Huerre, ''Perturbed free shear layers,'' Annu. Rev. Fluid Mech. **16**, 365 (1984).
[3]A. K. M. F. Hussain, ''Coherent structures and turbulence,'' J. Fluid Mech. **173**, 303 (1986).
[4]L. M. Mack, ''Linear stability theory and the problem of supersonic boundary-layer transition,'' AIAA J. **13**, 278 (1975).
[5]D. W. Bogdanoff, ''Compressibility effects in turbulent shear layers,'' AIAA J. **21**, 926 (1983).
[6]D. Papamoschou and A. Roshko, ''The compressible turbulent shear layer: An experimental study,'' J. Fluid Mech. **197**, 453 (1988).
[7]G. S. Elliott and M. Samimy, ''Compressibility effects in free shear layers,'' Phys. Fluids A **2**, 1231 (1990).
[8]S. G. Goebel and J. C. Dutton, ''Experimental study of compressible turbulent mixing layers,'' AIAA J. **29**, 538 (1991).
[9]N. T. Clemens and M. G. Mungal, ''Two- and three-dimensional effects in the supersonic mixing layer,'' AIAA J. **30**, 973 (1992).
[10]H. Gropengiesser, ''Study of the stability of boundary layers,'' NASA TT-F-12, 786 (1970).
[11]S. K. Lele, ''Direct numerical simulation of compressible free shear flows,'' AIAA-89-0375 (1989).
[12]N. D. Sandham and W. C. Reynolds, ''Three dimensional simulations of large eddies in the compressible mixing layer,'' J. Fluid Mech. **224**, 133 (1991).
[13]R. J. Gathmann, M. Si-Ameur, and F. Mathey, ''Numerical simulations of three-dimensional natural transition in the compressible confined shear layer,'' Phys. Fluids A **5**, 2946 (1993).
[14]P. E. Dimotakis, ''Two-dimensional shear-layer entrainment,'' AIAA J. **24**, 1791 (1986).
[15]D. K. McLaughlin, G. D. Morrison, and T. R. Troutt, ''Experiments on the instability waves in a supersonic jet and their acoustic radiation,'' J. Fluid Mech. **69**, 73 (1975).
[16]D. Papamoschou, ''Structure of the compressible turbulent shear layer,'' AIAA-89-0216, 1989.
[17]D. C. Fourguette, R. W. Dibble, and M. G. Mungal, ''Time evolution of the shear layer of a supersonic axisymmetric jet at matched conditions,'' AIAA J. **10**, 157 (1990).
[18]J. L. Hall, P. E. Dimotakis, and H. Rosemann, ''Experiments in non-reacting compressible shear layers,'' AIAA J. **31**, 2247 (1993).
[19]T. L. Jackson and C. E. Grosch, ''Inviscid spatial stability of a compressible mixing layer,'' J. Fluid Mech. **208**, 609 (1989).
[20]C. K. W. Tam and F. Q. Hu, ''On the three families of instability waves of high-speed jets,'' J. Fluid Mech. **201**, 447 (1989).
[21]G. S. Elliott, M. Samimy, and S. A. Arnette, ''The characteristics and evolution of large-scale structures in compressible mixing layers,'' Phys. Fluids **7**, 864 (1995).
[22]J. M. Seitzman, M. F. Miller, T. C. Island, and R. K. Hanson, ''Double-pulse imaging using simultaneous OH/acetone PLIF for studying the evolution of high-speed, reacting mixing layers,'' *Proceedings of the 25th International Symposium on Combustion*, July 31–August 5 1994, Irvine, CA.
[23]A. Lozano, B. Yip, and R. K. Hanson, ''Acetone: a tracer for concentration measurements in gaseous flows by planar laser-induced fluorescence,'' Exp. Fluids **13**, 369 (1992).
[24]D. Papamoschou and A. Bunyajitradulya, ''Double-exposure PLIF imaging of compressible shear layers,'' AIAA-95-0513, 1995.
[25]R. E. Breidenthal, ''Sonic eddy-a model for compressible turbulence,'' AIAA J. **30**, 101 (1993).
[26]D. Papamoschou and S.K. Lele, ''Vortex-induced disturbance field in a compressible shear layer,'' Phys. Fluids A **5**, 1412 (1993).
[27]D. Virk, F. Hussain, and R. M. Kerr, ''Compressible vortex reconnection,'' J. Fluid Mech. **304**, 47 (1995).
[28]D. Papamoschou, ''Thrust loss due to supersonic mixing,'' AIAA J. Prop. Power **10**, 804 (1994).
[29]P. E. Dimotakis, ''Turbulent free-shear layer mixing and combustion,'' Prog. Astro. Aero. **137**, 265 (1991).
[30]J. A. B. Wills, ''On convection velocities in turbulent shear flows,'' J. Fluid Mech. **20**, 417 (1964).
[31]T. R. Oakley, E. Loth, and R. J. Adrian, ''Cinematic particle image velocimetry of high-Reynolds-number turbulent free shear layers,'' AIAA J. **34**, 299 (1996).
[32]M. Nagai, ''Mechanism of pseudo-shock wave in supersonic jet,'' Bull. JSME **26**, 207 (1983).
[33]J. M. Seiner and E. Krejsa, ''Supersonic jet noise and the high speed civil transport,'' AIAA 89-2358 (1989).